

A new multisource and high-frequency approach to measuring $\delta^2\text{H}$ and $\delta^{18}\text{O}$ in hydrological field studies

Luke A. Pangle,¹ Julian Klaus,^{2,3} Elena S. F. Berman,⁴ Manish Gupta,⁴ and Jeffrey J. McDonnell^{2,5}

Received 10 April 2013; revised 6 October 2013; accepted 10 October 2013; published 20 November 2013.

[1] Measurements of $\delta^2\text{H}$ and $\delta^{18}\text{O}$ in isotope-based field studies have fundamentally improved our understanding of water flow and transport time scales in soils and headwater catchments. Until recently, however, technical constraints have limited the temporal resolution at which water samples could be collected and analyzed. We introduce a new sample acquisition system—consisting of a four-channel peristaltic pump, custom flow manifold, and CTC LCPAL auto-sampler—that is paired with a field-deployable laser spectrometer (LGR LWIA). Our system enables high-frequency (subhourly) measurement of $\delta^2\text{H}$ and $\delta^{18}\text{O}$ in as many as four water sources. We deployed the system at a field site in Corvallis, OR, USA, where we measured the $\delta^2\text{H}$ and $\delta^{18}\text{O}$ composition of precipitation and the drainage from two lysimeters. The system produced $\delta^2\text{H}$ and $\delta^{18}\text{O}$ time series for precipitation and drainage from each lysimeter at a temporal frequency of one sample every 34 min, which, on average, corresponded to 0.84, 0.63, and 0.48 mm of precipitation or lysimeter drainage per sample. The high-frequency data showed substantially greater short-term variability than observed when sampling at successively longer time intervals. The system and sampling configuration are versatile and can be adapted to sample multiple water flows at variable frequencies depending on the characteristic transit times of each source.

Citation: Pangle, L. A., J. Klaus, E. S. F. Berman, M. Gupta, and J. J. McDonnell (2013), A new multisource and high-frequency approach to measuring $\delta^2\text{H}$ and $\delta^{18}\text{O}$ in hydrological field studies, *Water Resour. Res.*, 49, 7797–7803, doi:10.1002/2013WR013743.

1. Introduction

[2] Measurements of $\delta^2\text{H}$ and $\delta^{18}\text{O}$ in isotope-based field studies have fundamentally improved our understanding of water flow and transport time scales in soils and headwater catchments. During the past 20 years, researchers have increased the frequency at which water samples are collected and analyzed for their stable-isotope composition (Table 1), but manual sampling at high frequency is extremely laborious to sustain, whereas automated sampling at high frequency quickly exceeds the storage capacity of conventional auto-sampling devices. Recent work has focused on instrument development to automate high-frequency isotope sampling and simultaneous analysis [Brand *et al.*, 2009; Lis *et al.*, 2008] to meet the demand

for more information-rich time series for hydrological applications [Kirchner *et al.*, 2004].

[3] Berman *et al.* [2009] utilized a field-deployable laser spectrometer to measure $\delta^2\text{H}$ and $\delta^{18}\text{O}$ in both precipitation and streamflow at a subhourly temporal resolution (40 samples/day from each source) during multiple storm events that spanned 4 weeks. In another application, they measured the isotopic composition of effluent from a melting snow core at a temporal resolution of more than 20 samples/h. Berman *et al.* [2009] used a liquid-water isotope analyzer that directly sampled the liquid-water sources and used a heated injection cell to volatilize the liquid water before measuring its absorption spectrum.

[4] Koehler and Wassenaar [2011] and Munksgaard *et al.* [2011] demonstrated a second approach, where a liquid-water source was brought into isotopic equilibrium with a stream of initially dry air. The air and resulting water vapor (that evaporated from the liquid-water source) were then pumped into the optical cavity of a laser spectrometer and the $\delta^2\text{H}$ and $\delta^{18}\text{O}$ were measured at intervals of a few seconds, though both studies reported that precision was improved by averaging these measurements over a period of 2–2.5 min [Koehler and Wassenaar, 2011; Munksgaard *et al.*, 2011]. These studies utilized water-vapor isotope analyzers that directly sampled water vapor that evaporated from the liquid-water source of interest. The isotopic composition of the liquid water was then calculated using the measured $\delta^2\text{H}$ and $\delta^{18}\text{O}$ of the vapor and temperature-dependent equilibrium-fractionation factors. Hence, the validity of this approach depends on constant maintenance

¹Water Resources Graduate Program, Oregon State University, Corvallis, Oregon, USA.

²Global Institute for Water Security, University of Saskatchewan, Saskatoon, Saskatchewan, Canada.

³Centre de Recherche Public—Gabriel Lippmann, Department of Environment and Agro-Biotechnologies, Belvaux, Luxembourg.

⁴Los Gatos Research, Mountain View, California, USA.

⁵School of Geosciences, University of Aberdeen, Aberdeen, Scotland, UK.

Corresponding author: L. A. Pangle, University of Arizona—Biosphere 2, Marshall Building, Rm. 526, 845 N. Park Ave., PO Box 210158-B, Tucson, AZ 85721-0158, USA. (lpangle@email.arizona.edu)

Table 1. The Time Intervals at Which Precipitation and Outflow Were Sampled for Isotope Analysis in a Selection of Recent Studies That Utilized Isotope-Based Hydrograph Separation Techniques^a

Reference	Precipitation Sample Interval (min mm)	Outflow Sample Interval (min)
<i>Birkel et al.</i> [2012]	1440 na	240
<i>Klaus et al.</i> [2013]	na ^b	5–30
<i>Liu et al.</i> [2011]	120 na	120–240
<i>Meriano et al.</i> [2011]	na ^c	2–480 ^c
<i>Hrachowitz et al.</i> [2011]	1440 na	≈60–120
<i>McGuire and McDonnell</i> [2010]	na 4.4	120–240
<i>Iwagami et al.</i> [2010]	na 10	60
<i>Vidon and Cuadra</i> [2010]	na ^c	60–120 ^d
<i>Gomi et al.</i> [2010]	na	30

^aThe sampling interval for precipitation is expressed per unit time, or accumulated flux.

^bUsed an irrigation water source that had a consistent isotopic composition.

^cA single bulk precipitation sample was used. Outflow sampling was most frequent during peak flow and less frequent during recession flow.

^dA single bulk precipitation sample was used. Each outflow sample was a mixture of three samples collected at 20 min intervals.

of isotopic equilibrium between the liquid-water source and the dry-air stream. Several devices have been used to achieve this equilibrium [*Herbstritt et al.*, 2012; *Koehler and Wassenaar*, 2011; *Munksgaard et al.*, 2011].

[5] The water-vapor isotope analyzers and liquid-vapor equilibration technique enabled greater sampling frequency than the liquid-water isotope analyzer, yet the latter method may be more robust for field deployment for several reasons. Foremost, the liquid analyzer volatilizes the sample water using a heated injection cell, whereas the liquid-vapor equilibration technique relies on an ancillary device (e.g., a marble-filled jar) where constant isotopic equilibrium must be maintained between the continuously flowing liquid source and a stream of dry air through evaporation at the ambient temperature. This equilibrium condition is potentially sensitive to temperature fluctuations in the incoming water and air streams (*Munksgaard et al.*, 2011; though less sensitivity was reported by *Koehler and Wassenaar* [2011]), and some of the devices used for this purpose may alter the temperature dependence of equilibrium-isotope fractionation [*Herbstritt et al.*, 2012; *Koehler and Wassenaar*, 2011].

[6] Second, as demonstrated by *Berman et al.* [2009], the field-deployable liquid-water isotope analyzer enables automated measurements of multiple external standards throughout the period of analysis. Standard curves that envelop the full range of anticipated isotope concentrations in the sample source can be developed at regular time intervals and allow for correction of errors associated with instrument drift. Laboratory studies that applied the liquid-vapor equilibration method lacked a procedure for automated measurements of standards [*Herbstritt et al.*, 2012; *Koehler and Wassenaar*, 2011]. While measuring the isotopic composition of precipitation, *Munksgaard et al.* [2011] partially addressed this problem with an automated system that periodically sampled from a *single* reference water source when the precipitation ceased, then collected samples of the reference water daily to verify its isotopic composition using mass spectrometry.

[7] Last, the liquid-water analyzer evacuates the optical cavity after each measurement, which helps to minimize the confounding influence of residual water vapor on subsequent measurements (i.e., the carryover effect). This carryover effect may be more problematic for continuous measurement of a stream of water vapor. For example, *Munksgaard et al.* [2011] showed that an equilibration period of 7–8 min was required when consecutively sampling source waters with different isotope compositions (notably *Koehler and Wassenaar* [2011] reported shorter equilibration times—on the order of 30 s).

[8] Here, we introduce a new sample acquisition system that is combined with an upgraded version of the field-deployable liquid-water isotope analyzer introduced by *Berman et al.* [2009]. The new sample acquisition system and instrument advance our current high-frequency and field-deployable sampling capabilities by (1) increasing the number of water sources that can be sampled from disparate locations and across head gradients, (2) utilizing updated vaporization and gas conductance features in the laser spectrometer to abbreviate the time per sample measurement, and (3) reducing the frequency of required maintenance. The objectives of this study were to show proof of concept by deploying this system at a field site where water from three sources is sampled and analyzed at a subhourly frequency, and to compare the short-term dynamics of the high-frequency isotope data with data collected at coarser temporal resolution.

2. Materials and Methods

2.1. Sample Acquisition System and Field-Deployable Laser Spectrometer

[9] The new sample acquisition system combined a four-channel peristaltic pump and a four-port stainless-steel sampling manifold that was mounted on a CTC LCPAL auto-sampler tray (Figure 1). The peristaltic pump (Ismatec MS-CA Stand-mounted Pump) had a fixed-speed motor and eight rollers that turned on the drive shaft at 20 rpm. The maximum pressure differential created by the pump was up to 100 kPa depending on the type of compressible tubing used. We used PharMed Ismaprene compressible tubing (1.65 mm inside diameter) with vinyl tubing (9.5 mm inside diameter) connected to the intake and output sides of the compressible tubing to deliver water from the discharge point to the sampling manifold. The pump sustained consistent flow rates of 5.56–5.72 mL min⁻¹ depending on the length of the particular sample line and the total head gradient.

[10] The custom manifold was designed to attach to the tray holder of a CTC LCPAL auto-sampler (Figure 1). Water flowed vertically through the base of the manifold through four vertical stainless steel tubes. The top of the manifold had a Plexiglas cover with drilled openings above each tube that allowed the 1.2 μL syringe to draw from the inflowing water, while also preventing debris from falling into the sample tray. The slanted interior of the stainless steel manifold allowed the water to drain out of an attached waste line. This design prevented the accumulation of any residual water within the four tubes, which reduced the risk of particle matter accumulation that could cause the injection syringe to malfunction. The moving arm of the LCPAL

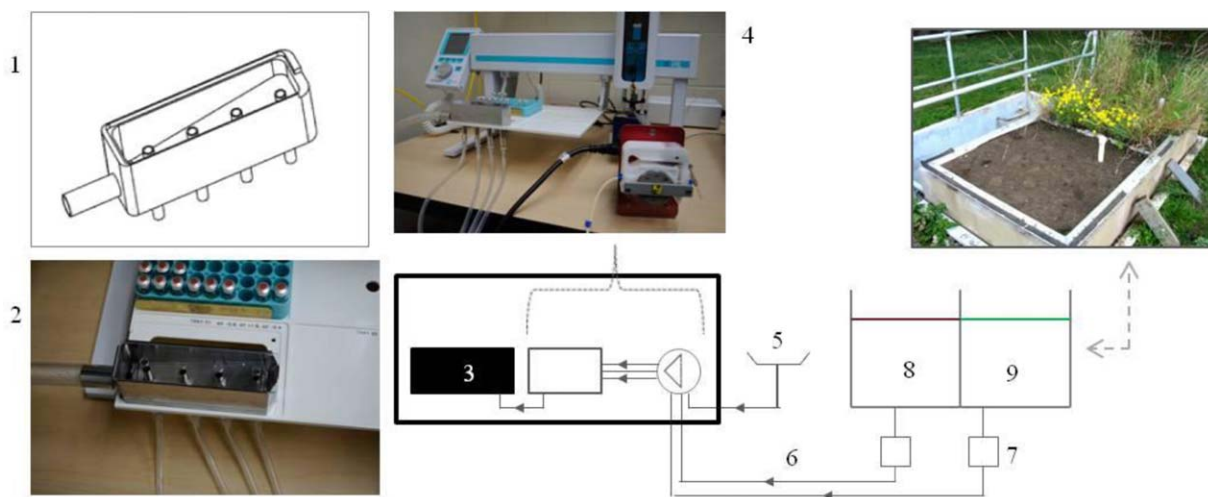


Figure 1. Diagram illustrating the components of the new sample-acquisition system and site of field deployment: (1) sketch of the custom manifold, (2) photo of manifold mounted to sample tray of a CTC LCPAL auto-sampler, with four incoming sample lines and outgoing waste line, (3) Liquid Water Isotope Analyzer (LGR), (4) photograph illustrating the flow path from the four-channel peristaltic pump to the sample inflow ports on the base of the manifold, (5) precipitation collector, (6) vinyl tubing connecting each water source to the peristaltic pump, (7) tipping bucket gages, (8) lysimeter with bare soil surface, and (9) lysimeter with grassland vegetation.

auto-sampler was calibrated to locate the horizontal and vertical positions of each inlet tube.

[11] The ratio of $^2\text{H}/^1\text{H}$ and $^{18}\text{O}/^{16}\text{O}$ in liquid water samples was measured with a Los Gatos Research (LGR) liquid-water isotope analyzer (LWIA 24d), and converted to $\delta^2\text{H}$ and $\delta^{18}\text{O}$ relative to Vienna Standard Mean Ocean Water (VSMOW). We used a sampling scheme that included three external standards interleaved with nine samples. Table 2 shows the sampling sequence: there were five injections of external standard 1 (standards were contained in vials on the sample tray), followed by five injections from each of the three water sources. The first two injections of each standard and water source were omitted to account for the carryover effect that results from traces of residual vapor molecules from the previous sample remaining in the cavity, and the last three injections were averaged. Each water injection required 102 s—the time required to evacuate gas from the measurement cell, inject and subsequently remove dry air, inject and volatilize the new liquid-water sample, and measure absorption spectrum (a quicker version of the instrument described by *Berman et al.* [2009]). This scheme enabled one sample (the average of the last three injections) to be analyzed from each of three water sources every 34 min (including the time required for measuring the standard). The three injections were not drawn from exactly the same volume of water, since the water flow through the manifold was continuous but the LCPAL auto-sampler withdrew discrete volumes from this continuous stream. Hence, the $\delta^2\text{H}$ and $\delta^{18}\text{O}$ values for each individual sample represent an average of three discrete samples drawn from approximately 29 mL of water (considering an average pump rate of 5.6 mL/min over the 306 s required to measure three water injections). Second and third iterations of this sequence (Table 2) each used unique external standards (standards 2 and 3), which

yielded a three-point standard curve every 102 min. The analytical accuracy was determined by the accuracy of the external standards, which was reported as ± 1 and 0.2‰ for $\delta^2\text{H}$ and $\delta^{18}\text{O}$, respectively. The precision was 0.36 and 0.07‰ for $\delta^2\text{H}$ and $\delta^{18}\text{O}$, respectively—quantified as one standard deviation of all measured external standard values.

2.2. Field Deployment

[12] We deployed the sample acquisition system and LWIA at a lysimeter study site at the Terracosm Research Facility in Corvallis, OR, USA (44.57°N , -123.29°W ; 77 m elevation) during March 2012. The instrumentation was placed inside acrylic boxes to protect it from dust and humidity and located inside an uninsulated shed with 120 VAC power. We measured $\delta^2\text{H}$ and $\delta^{18}\text{O}$ in the drainage (R) from two nonweighing lysimeters—one with a bare soil surface and the other with a grassland community. Each lysimeter had a volume of 1 m^3 ($1 \times 1 \times 1\text{ m}$) and was filled with a silty clay loam soil. The R from each lysimeter

Table 2. The Sequence of External-Standard and Water-Sample Measurements Performed by the Auto-Sampler and Liquid Water Isotope Analyzer^a

Source	Number of Injections	Time Required (s)
Standard	5	510
Lysimeter (bare soil)	5	510
Lysimeter (grassland)	5	510
Precipitation	5	510

^aFive injections of each source were analyzed; data from the first two injections were discarded to account for sample carryover. Three unique standards were used, yielding a three-point standard curve every 102 min of run time.

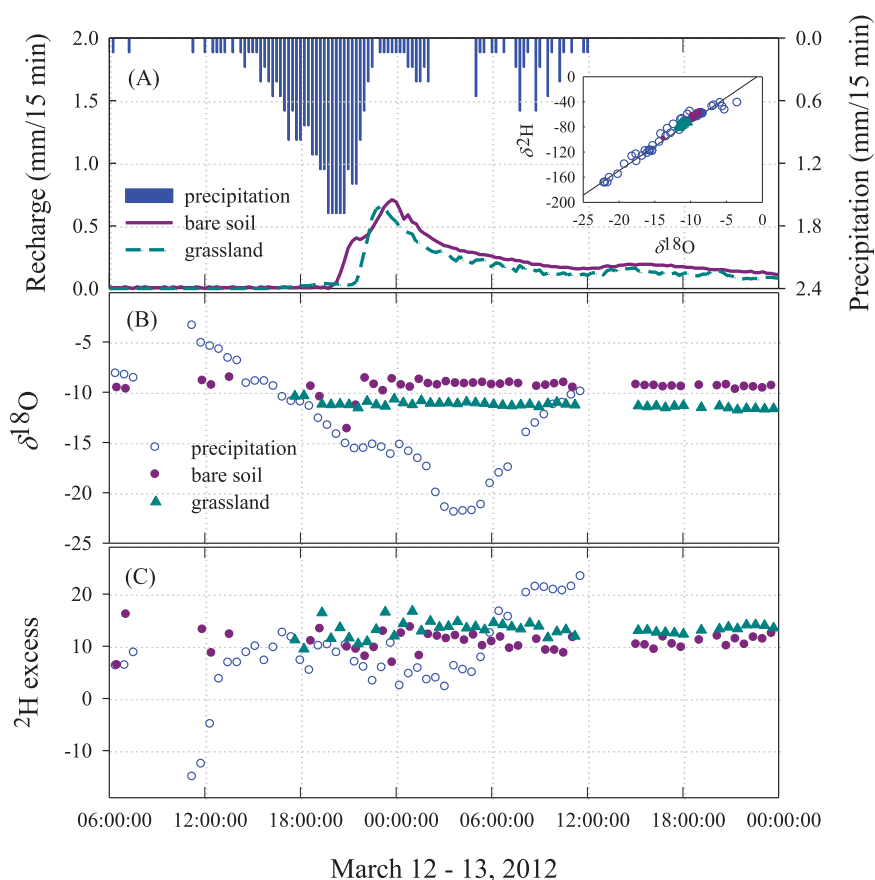


Figure 2. (a) Time series of precipitation, P , and drainage, R , from the lysimeters with bare soil surface, R_{bs} , and grassland vegetation, R_g . The flux data are presented as 15 min totals. The inset shows the dual isotope plot with event-specific meteoric water line ($\delta^2\text{H} = 7.81\delta^{18}\text{O} + 5.98$). (b) Time series of $\delta^{18}\text{O}$ in P , R_{bs} , and R_g . The sampling frequency was one sample every 34 min, with missing data points in some instances. (c) Time series of deuterium excess in each water source, calculated as $\delta^2\text{H} - 8 \cdot \delta^{18}\text{O}$.

was measured with a tipping-bucket gage and HOBO event logger (Onset Computer Corporation, Inc., Bourne, MA). A funnel was attached to the base of each tipping bucket that directed the water flow into a closed container (0.040 L volume) that was connected to the sample acquisition system by the vinyl tubing (Figure 1). The lengths of vinyl tubing ranged from 13 to 18 m, and if completely full, held 0.92–1.28 L of water. It is possible that the distinct isotope composition of small parcels of water could be influenced by diffusive mixing with adjacent water parcels within the vinyl tubing. However, this effect is likely negligible since the self-diffusion coefficients of H^2HO and H_2^{18}O in H_2O are on the order of $10^{-9} \text{ m}^2 \text{ s}^{-1}$ [Longworth, 1960]. This assumption could be tested in future applications by pumping water sequentially from two sources with known and different isotopic compositions and measuring any deviation that might result due to mixing within the tubing. The time stamp associated with each isotope measurement was corrected based on the known travel time of the water within the vinyl tubing. We constructed a rainfall collector with a circular orifice of 68 cm diameter to route precipitation to the sample acquisition system. Another tipping bucket gage was used to measure precipitation amount (P)

at a location that was approximately 580 m southeast of the lysimeter study site.

[13] We used data from a March 2012 storm event (occurring from 12 March to 13 March) to compare the short-term variations in $\delta^{18}\text{O}$ and $\delta^2\text{H}$ observed in the high-frequency data with those observed within time series collected at 2 and 3 h intervals. The latter two data sets were generated by subsampling data points from the high-frequency time series. These subsampled data sets emulate the time series of data that would have resulted from grab sampling at 2 and 3 h intervals (exemplary of the range of sampling frequencies noted in Table 1).

3. Results

[14] Total P during the 12–13 March storm event was 39 mm and caused 29 and 22 mm of R from the bare soil (R_{bs}) and grassland lysimeters (R_g), respectively (Figure 2a). The sample-acquisition system and LWIA enabled the collection and analysis of 46, 46, and 45 samples of P , R_{bs} , and R_g , respectively, resulting in an average of 0.84, 0.63, and 0.48 mm of accumulated flux per sample (Figures 2a and 2b). The $\delta^{18}\text{O}$ values ranged by 18.56, 5.12, and 1.41‰ for

Table 3. The Maximum Rate of Change in $\delta^{18}\text{O}$ and $\delta^2\text{H}$ (Calculated as the Slope Between Consecutive Data Points) Observed in the High-Frequency Data and Data Sets That Were Subsampled From the High-Frequency Series at 2 and 3 h Intervals

Frequency (min)	max $d(\delta^2\text{H})/dt$ (‰ min^{-1})			max $d(\delta^{18}\text{O})/dt$ (‰ min^{-1})		
	P	R_{bs}	R_{g}	P	R_{bs}	R_{g}
34	38.0	35.9	9.9	4.6	4.8	1.5
120	24.0	17.0	3.0	2.6	1.9	0.75
180	22.8	10.5	1.2	2.3	1.8	0.75

P , R_{bs} , and R_{g} , respectively (Figure 2b). The corresponding range among $\delta^2\text{H}$ values was 127.32, 43.43, and 10.08 ‰ (data not shown). The $\delta^{18}\text{O}$ and $\delta^2\text{H}$ values in P were related by an event-specific meteoric-water line (Figure 2a inset; $\delta^2\text{H} = 7.81\delta^{18}\text{O} + 5.98$), and the delta values in R_{bs} and R_{g} fell closely along this line. The simultaneous measurement of $\delta^{18}\text{O}$ and $\delta^2\text{H}$ enabled calculated time series of deuterium excess that ranged by 38.41, 9.70, and 7.24 ‰ in P , R_{bs} , and R_{g} , respectively (Figure 2c).

[15] The accumulated flux per sample varied depending on rates of P and R . For example, from 19:00 to 21:00 on 12 March, the frequency was 3.0 mm/sample for P ; from 22:00 to 2:00 the frequency was 1.3 and 1.1 mm/sample for R_{bs} and R_{g} , respectively. Prior to the R response at 20:00, there was intermittent and low flow from the bare-soil lysimeter that was sufficient to be sampled in a few instances (Figure 2b, 6:00–18:00). From 11:00 to 15:00 on 13 March there was a rapid reduction in cloudiness and increase in air temperature that caused a corresponding increase in the operating temperature of the LWIA. Samples were omitted during this period in accord with the quality-control metrics included in the LGR postprocessing software. Also, $\delta^{18}\text{O}$ and $\delta^2\text{H}$ measurements were taken during 3:00–5:00 on 13 March when no P was measured by the tipping bucket (Figures 2a and 2b). These data points may have resulted from small amounts of rain that were collected and measured by the sample acquisition system and LWIA, but were insufficient to generate a tip of the tipping bucket (since the catchment area of the rainfall-sample collector was greater than the tipping bucket by a factor of seven). It is also possible that some debris accumulated at the tubing connection to the rainfall collector, which may have partially constricted and delayed the flow of precipitation into the tubing (this was observed on one other occasion).

[16] Our new system yielded time series of $\delta^{18}\text{O}$ and $\delta^2\text{H}$ that showed fine-scale temporal dynamics that were unapparent when sampling less frequently. The maximum rates of change between isotope values in the high-frequency data sets were two to three times greater than observed in the data sets that were subsampled at 2 and 3 h intervals (Table 3), which highlights the increased short-term dynamics that can be observed when sampling at greater frequency.

4. Discussion

4.1. System Performance

[17] The new sample acquisition system was capable of producing time series of $\delta^{18}\text{O}$ and $\delta^2\text{H}$ (and thus deuterium

excess) at subhourly temporal resolution from three different water sources. A fourth source could be readily added with the present system. This system benefitted from upgrades to the liquid vaporization and gas conductance mechanisms employed by the LWIA, resulting in a 15% reduction in the injection time as compared to values reported by *Berman et al.* [2009]. Further, the vastly reduced water-pump rate (from 1.86 to 0.006 L min^{-1}) reduced the transport of sediment into the manifold and negated the need for regular maintenance of a filtration system. However, filters could be added in-line with the sample tubing when sampling more turbulent waters. During this deployment the instrumentation operated without maintenance for more than two days (2455 total injections). The sample transfer line and injection block need to be cleaned at a 5–10 days interval under continuous operation, which only requires 1–2 h of instrument down-time given a second injection block that can be readily swapped into operation.

[18] The key requisite for utilizing the new sample acquisition system and LWIA for field deployment is a nearby power supply, which may be a limiting factor for researchers working in remote locations without nearby power lines. We stored the laser spectrometer in a structure with no climate control—noninsulated walls with open air circulation at doors and translucent wall paneling—but experienced only marginal data loss due to temperature fluctuations. A small fabricated shed (similar to those often used to store automated water samplers) would be practical to transport to a field site and would improve ambient temperature regulation. Additionally, new models of the LWIAs have internal-temperature-control mechanisms that would eliminate data omission due to temperature fluctuations like we experienced on 13 March.

4.2. Possibilities for Further Field Applications

[19] Our system opens up new possibilities for in situ field analysis of ^{18}O and $\delta^2\text{H}$ in multiple water sources. In addition to lysimeter studies, at least three possible field applications of this system are immediately apparent.

[20] First, the multisource sampling capability could be utilized to quantify the characteristic time scales of multiple sources of streamflow [*McGuire and McDonnell*, 2010] by simultaneously sampling precipitation and streamflow, along with groundwater seeps and/or snow-melt lysimeters. Sampling from overland-flow collectors could also be possible, though including filter devices in the sample line would be important for this water source. Overland flow may also contain high levels of organic molecules that can affect the measured absorption spectrum [*West et al.*, 2010], though this problem can now be ameliorated using additional postprocessing software that identifies sample measurements that were compromised by the presence of organics [*West et al.*, 2011], and can be used to correct the contaminated measurements [*Schultz et al.*, 2011].

[21] Second, this system could illuminate how canopy interception and mixing processes alter the isotopic composition of effective precipitation that eventually infiltrates the soil and generates streamflow. Arrays of large tarps and streamflow collectors could be arranged to drain to single storage devices, thus providing spatially integrated flows of throughfall and streamflow that could be sampled at high

frequency along with precipitation. High-frequency data may be more valuable for some water sources than others. The sampling configuration can be readily adjusted to sample the more dynamic sources more frequently and vice versa.

[22] Last, the multisource and high-frequency capabilities of this system could advance current research that utilizes stable isotopes to quantify transit times in soils and hillslopes [McGuire and McDonnell, 2010; Stumpp et al., 2009] and catchments [Birkel et al., 2010; Broxton et al., 2009; McGuire et al., 2005; Soulsby et al., 2011]. As previously indicated [Birkel et al., 2010], it can be difficult or impossible to identify a definitive transit-time distribution, or analyze the time variance of the distribution, if the time series of tracer concentration in the outflow shows little variation. Although the analysis of transit-time distributions often requires multiyear data sets—likely a prohibitively long time to leave a laser spectrometer in the field—in many climatic regimes a field deployment spanning a few weeks could still capture the most dynamic periods of flow that control the shape and conditionality of the transit-time distribution describing the system (e.g., in areas with snow-melt dominated runoff regimes or monsoonal rain systems [Heidbüchel et al., 2012]).

5. Conclusions

[23] Our system includes three key advancements for field-deployable high-frequency sampling and analysis of stable isotopes in water:

[24] 1. Expanded number of water sources that can be automatically sampled and analyzed.

[25] 2. Increased sampling frequency via reduced time required per sample injection.

[26] 3. Improved pump and manifold design that minimizes debris transport into the system and reduces the frequency of required maintenance.

[27] The time and effort required for installation and maintenance are comparable to that required for traditional automatic-water-sampling equipment, and the real-time on-site analysis results in a net time savings since sample retrieval, pipetting, and in-lab analysis are negated. Our proof of concept example in this paper shows how greater sampling frequency enhances the observable dynamics in a stable-isotope data set.

[28] **Acknowledgments.** This research was supported by DOE SBIR grant DE-FG02-08ER84976. We thank Jillian Gregg of Terrestrial Ecosystems Research Associates for site access and assistance. We thank Tina Garland and Caroline Patrick for assistance with field work.

References

Berman, E. S. F., M. Gupta, C. Gabrielli, T. Garland, and J. J. McDonnell (2009), High-frequency field-deployable isotope analyzer for hydrological applications, *Water Resour. Res.*, *45*, W10201, doi:10.1029/2009WR008265.

Birkel, C., S. M. Dunn, D. Tetzlaff, and C. Soulsby (2010), Assessing the value of high-resolution isotope tracer data in the stepwise development of a lumped conceptual rainfall-runoff model, *Hydrol. Processes*, *24*(16), 2335–2348, doi:10.1002/hyp.7763.

Birkel, C., C. Soulsby, D. Tetzlaff, S. Dunn, and L. Spezia (2012), High-frequency storm event isotope sampling reveals time-variant transit time distributions and influence of diurnal cycles, *Hydrol. Processes*, *26*(2), 308–316, doi:10.1002/hyp.8210.

Brand, W. A., H. Geilmann, E. R. Crosson, and C. W. Rella (2009), Cavity ring-down spectroscopy versus high-temperature conversion isotope ratio mass spectrometry: A case study on delta H-2 and delta O-18 of pure water samples and alcohol/water mixtures, *Rapid Commun. Mass Spectrom.*, *23*(12), 1879–1884, doi:10.1002/rcm.4083.

Broxton, P. D., P. A. Troch, and S. W. Lyon (2009), On the role of aspect to quantify water transit times in small mountainous catchments, *Water Resour. Res.*, *45*, W08427, doi:10.1029/2008WR007438.

Gomi, T., Y. Asano, T. Uchida, Y. Onda, R. C. Sidle, S. Miyata, K. Kosugi, S. Mizugaki, T. Fukuyama, and T. Fukushima (2010), Evaluation of storm runoff pathways in steep nested catchments draining a Japanese cypress forest in central Japan: A geochemical approach, *Hydrol. Processes*, *24*(5), 550–566, doi:10.1002/hyp.7550.

Heidbüchel, I., P. A. Troch, S. W. Lyon, and M. Weiler (2012), The master transit time distribution of variable flow systems, *Water Resour. Res.*, *48*, W06520, doi:10.1029/2011WR011293.

Herbsttritt, B., B. Gralher, and M. Weiler (2012), Continuous in situ measurements of stable isotopes in liquid water, *Water Resour. Res.*, *48*, W03601, doi:10.1029/2011WR011369.

Hrachowitz, M., R. Bohte, M. L. Mul, T. A. Bogaard, H. H. G. Savenije, and S. Uhlenbrook (2011), On the value of combined event runoff and tracer analysis to improve understanding of catchment functioning in a data-scarce semi-arid area, *Hydrol. Earth Syst. Sci.*, *15*(6), 2007–2024, doi:10.5194/hess-15-2007-2011.

Iwagami, S., M. Tsujimura, Y. Onda, J. Shimada, and T. Tanaka (2010), Role of bedrock groundwater in the rainfall-runoff process in a small headwater catchment underlain by volcanic rock, *Hydrol. Processes*, *24*(19), 2771–2783, doi:10.1002/hyp.7690.

Kirchner, J. W., X. H. Feng, C. Neal, and A. J. Robson (2004), The fine structure of water-quality dynamics: The (high-frequency) wave of the future, *Hydrol. Processes*, *18*, 1353–1359, doi:10.1002/hyp.5537.

Klaus, J., E. Zehe, M. Elsner, C. Kulls, and J. J. McDonnell (2013), Macropore flow of old water revisited: Experimental insights from a tile-drained hillslope, *Hydrol. Earth Syst. Sci.*, *17*, 103–118, doi:10.5194/hess-17-103-2013.

Koehler, G., and L. I. Wassenaar (2011), Realtime stable isotope monitoring of natural waters by parallel-flow laser spectroscopy, *Anal. Chem.*, *83*(3), 913–919, doi:10.1021/ac102584q.

Lis, G., L. I. Wassenaar, and M. J. Hendry (2008), High-precision laser spectroscopy D/H and O-18/O-16 measurements of microliter natural water samples, *Anal. Chem.*, *80*(1), 287–293, doi:10.1021/ac701716q.

Liu, W. J., W. Y. Liu, H. J. Lu, W. P. Duan, and H. M. Li (2011), Runoff generation in small catchments under a native rain forest and a rubber plantation in Xishuangbanna, southwestern China, *Water Environ. J.*, *25*(1), 138–147, doi:10.1111/j.1747-6593.2009.00211.x.

Longworth, L. G. (1960), The mutual diffusion of light and heavy water, *J. Phys. Chem.*, *64*(12), 1914–1917, doi:10.1021/j100841a028.

McGuire, K. J., and J. J. McDonnell (2010), Hydrological connectivity of hillslopes and streams: Characteristic time scales and nonlinearities, *Water Resour. Res.*, *46*, W10543, doi:10.1029/2010WR009341.

McGuire, K. J., and J. J. McDonnell, M. Weiler, C. Kendall, B. L. McGlynn, J. M. Welker, and J. Seibert (2005), The role of topography on catchment-scale water residence time, *Water Resour. Res.*, *41*, W05002, doi:10.1029/2004WR003657.

Meriano, M., K. W. F. Howard, and N. Eyles (2011), The role of mid-summer urban aquifer recharge in stormflow generation using isotopic and chemical hydrograph separation techniques, *J. Hydrol.*, *396*(1–2), 82–93, doi:10.1016/j.jhydrol.2010.10.041.

Munksgaard, N. C., C. M. Wurster, and M. I. Bird (2011), Continuous analysis of $\delta^{18}\text{O}$ and δD values of water by diffusion sampling cavity ring-down spectrometry: A novel sampling device for unattended field monitoring of precipitation, ground and surface waters, *Rapid Commun. Mass Spectrom.*, *25*(24), 3706–3712, doi:10.1002/rcm.5282.

Schultz, N. M., T. J. Griffis, X. H. Lee, and J. M. Baker (2011), Identification and correction of spectral contamination in $^2\text{H}/^1\text{H}$ and $^{18}\text{O}/^{16}\text{O}$ measured in leaf, stem, and soil water, *Rapid Commun. Mass Spectrom.*, *25*(21), 3360–3368, doi:10.1002/rcm.5236.

Soulsby, C., K. Piegat, J. Seibert, and D. Tetzlaff (2011), Catchment-scale estimates of flow path partitioning and water storage based on transit

- time and runoff modelling, *Hydrol. Processes*, 25(25), 3960–3976, doi:10.1002/hyp8324.
- Stumpp, C., P. Maloszewski, W. Stichler, and J. Fank (2009), Environmental isotope (δ O-18) and hydrological data to assess water flow in unsaturated soils planted with different crops: Case study lysimeter station “Wagna” (Austria), *J. Hydrol.*, 369(1–2), 198–208, doi:10.1016/j.jhydrol.2009.02.047.
- West, A. G., G. R. Goldsmith, P. D. Brooks, and T. E. Dawson (2010), Discrepancies between isotope ratio infrared spectroscopy and isotope ratio mass spectrometry for the stable isotope analysis of plant and soil waters, *Rapid Commun. Mass Spectrom.*, 24(14), 1948–1954, doi:10.1002/rcm.4597.
- West, A. G., G. R. Goldsmith, I. Matimati, and T. E. Dawson (2011), Spectral analysis software improves confidence in plant and soil water stable isotope analyses performed by isotope ratio infrared spectroscopy (IRIS), *Rapid Commun. Mass Spectrom.*, 25(16), 2268–2274, doi:10.1002/rcm.5126.
- Vidon, P., and P. E. Cuadra (2010), Impact of precipitation characteristics on soil hydrology in tile-drained landscapes, *Hydrol. Processes*, 24(13), 1821–1833, doi:10.1002/hyp.7627.